Article

A DFT Investigation on the Electronic Structures and Au Adatom Assisted Hydrogenation of Graphene Nanoflake Array

SONG Yang[1,2], TAO Lei[1], ZHANG Yanfang[1], PAN Jinbo[1,2] and DU Shixuan[1,2,3,4]✉

Received April 9, 2021
Accepted April 21, 2021

Graphene nanoribbons with zigzag edges(ZGNRs) have attracted much attention for their spin-polarized edge states predicted more than 15 years ago. Since the ZGNRs are fabricated on metal substrates using molecular precursors, due to their strong coupling with metal substrates, experimental detection of the spin-polarized edge states is still difficult. Here, we design a partially hydrogenated graphene(PHGr), in which periodic hexagonal graphene nanoflakes(GNFs) with zigzag boundaries are embedded in a hydrogenated graphene layer. Using density functional theory(DFT) based first-principles calculations, we find that the hexagonal GNFs exhibit spin-polarized boundary states at their opposite zigzag boundaries, which is similar with the bow-tie-shaped GNFs and ZGNRs. DFT calculations demonstrate that the PHGr is a semiconductor with an antiferromagnetic ground state. Moreover, the antiferromagnetic boundary states and semiconducting properties keep unchanged when the size of GNF varies from 1.4 nm to 2.3 nm. The robustness of the spin-polarized boundary states enables this PHGr as a robust material for detecting spin-polarized boundary states coming from zigzag boundaries. In addition, we find that single Au atoms selectively adsorbed on boundaries catalyze H_2 dissociation and therefore lower the barrier of graphene hydrogenation. Therefore, the PHGr can be used not only in carbon-based spintronic devices but also as a platform for single atom catalyst.

Keywords Graphene nanoflake; Hydrogenated graphene; Antiferromagnetic semiconductor; Single atom catalysis; Spintronics

1 Introduction

Graphene and derived nanostructures exhibit various novel electronic properties[1−4]. In the past decades, there was an increasing interest in theoretical investigations on magnetic properties in graphene-based materials. For example, zigzag graphene nanoribbons(ZGNRs) have a width-dependent band gap[5,6], and favor antiferromagnetic coupling between two opposite edges as ground state[7−9], that can result in half-metallicity when there is an in-plane homogeneous electric field[10]. The antiferromagnetic edge states are also predicted to occur in graphene nanoflake(GNF)[11,12]. Based on the benzenoid graph theory[13] and Lieb's theorem[14], GNFs in a specific shape have an antiferromagnetic order across the zigzag-edges[11]. The ZGNRs and GNFs with zero-energy edge states in antiferromagnetic ordering[11,12,15] are potential candidates for graphene-based spintronic devices.

For the synthesis of ZGNRs and GNFs in specific shapes, the most commonly used method is depositing molecule precursor onto metal substrates and then annealing at high temperature[16−18]. However, it's difficult to directly observe the antiferromagnetic edge states in fabricated ZGNRs/GNFs because of the electronic interaction between metal substrates and ZGNRs/GNFs[19]. To decouple the interaction from the metal substrate, several methods have been used in experiments. The edge-localized states with energy splitting in a ZGNR were observed by scanning tunneling spectroscopy after moving ZGNR from metal substrate onto an insulating layer, such as NaCl[16]. The edge states of a GNF with zigzag edges have been detected after silicon intercalation at the GNF-Ir(111) interface[20]. However, the antiferromagnetic properties of the edge states have not been observed in experiments. A density functional theory investigation demonstrates that C_2H_4 is the ideal terminal group for zigzag graphene nanoribbons (ZGNRs) in terms of preserving the edge magnetism with experimental feasibility[21]. Recently, it has been demonstrated that in the system of one-third-hydrogenated graphene on Ru(0001), the hydrogen atoms in hydrogenated graphene at the interface decouple the graphene from Ru substrate[22]. Therefore, it suggests that ZGNRs/GNFs surrounded by hydrogenated graphene can realize the spin-polarized edge states in ZGNRs and GNFs due to the decoupling effect of the surrounding hydrogenated graphene.

In this paper, we present an artfully designed hexagonal GNF arranged as a rhombic array and embedded in a hydrogenated graphene(graphane). The graphane region is

✉ DU Shixuan
sxdu@iphy.ac.cn
1. Institute of Physics and School of Physical Sciences, University of Chinese Academy of Sciences, Chinese Academy of Sciences, Beijing 100190, P. R. China;
2. Beijing National Laboratory for Condensed Matter Physics, Institute of Physics of Chinese Academy of Sciences, Beijing 100190, P. R. China;
3. CAS Center for Excellence in Topological Quantum Computation, Beijing 100190, P. R. China;
4. Songshan Lake Materials Laboratory, Dongguan 523808, P. R. China

https://doi.org/10.1007/s40242-021-1163-x

expected to make the hexagonal GNF decoupled from substrates in the future experiment. Using density-functional-theory(DFT) calculations, we demonstrate that the hexagonal GNF with zigzag boundaries have antiferromagnetic spin polarizations localized on two opposite boundaries. The periodic GNF array is semiconductor with an antiferro-magnetic ground state. The characteristics of the ferromagnetic distribution of electrons in GNFs are the same as those in isolated bow-tie-shaped GNFs. Moreover, the properties of antiferromagnetic and semiconducting properties retain when the width of GNF varies from 1.4 nm to 2.3 nm. Additionally, the partially hydrogenated graphene(PHGr) with a periodic GNF array is demonstrated as a template for selective adsorption of Au atoms. The single Au atom can be selectively adsorbed on an sp^2 carbon atom on the boundary. When a H_2 molecule is introduced in the system, it can be adsorbed on the Au adatom first. Further calculations show that the adsorbed Au adatom can be used as a catalyst for H_2 dissociation. The dissociated H atoms hydrogenate the neighboring sp^2 carbon atoms at a lower barrier comparing with that in a direct hydrogenation of graphene, exhibiting a great potential in controllable hydrogenation of graphene.

2 Calculation Method

All DFT calculations were perfor-med using projector-augmented wave(PAW)[23,24] pseudopo-tentials combined with the local-density-approximation(LDA) exchange-correlation functional as implemented in the Vienna *ab-initio* Simulation Package(VASP)[25,26]. The energy cutoff of the plane-wave basis was set to be 800 eV. All the partially hydrogenated graphene (PHGr) systems were modelled by (12×12) graphene supercells. The vacuum layers are all larger than 1.5 nm. All the models were relaxed until the force on each atom was smaller than 0.1 eV/nm and the energy was converged to 1×10^{-5} eV. The Brillouin zone was sampled by a (1×1×1) *Γ*-centered *k*-mesh[27].

The H_2 molecule adsorption and dissociation processes were simulated using the climbing-image nudged elastic band (CI-NEB) method[28,29]. Before performing CI-NEB calculations, the initial and final structures were fully relaxed until the residual force on each of the relaxed atoms was smaller than 0.5 eV/nm. Five intermediate states were constructed by using linear interpolation. The limit of force convergence was set to 1 eV/nm.

3 Results and Discussion

3.1 Atomic Structures of GNF Arrays

The structure of the partially hydrogenated graphene layer is displayed in Fig.1(A). It consists of two parts: honeycomb shaped fully hydrogenated graphene(graphane) and pristine graphene(graphene nanoflake, GNF). The black rhombus marks a primitive cell, a 12×12 graphene supercell(PHGr-12), with a lattice constant of a=2.95 nm. The structure details are in Fig.1(B). The GNF region is terminated with two kinds of zigzag boundaries, zigzag-1(ZZ-1, consisting of sp^2 and sp^3 carbon atoms) and zigzag-2(ZZ-2, consisting of sp^2 carbon atoms), marked by blue and red zigzag lines, respectively. The distance between two ZZ-1 boundaries is 2.3 nm(N=12). In graphane region, H atoms are adsorbed on both sides of graphene alternatively and are in pairs along the direction perpendicular to ZZ-1 boundary. We also show models with GNFs in small sizes: PHGr-10 and PHGr-8 in Fig.1(C) and (D). PHGr-10 and PHGr-8 have the same lattice constant with PHGr-12 as marked by the black rhombus, while have GNFs in different sizes marked by red and blue double-headed arrows. N is the number of zigzag carbon chains between two opposite ZZ-1 boundaries. For example, in PHGr-12, the width between two ZZ-1 boundaries is N=12, while the width between two ZZ-2 boundaries is N=11. In the following, we take PHGr-12 as an example to investigate the detailed electronic structures.

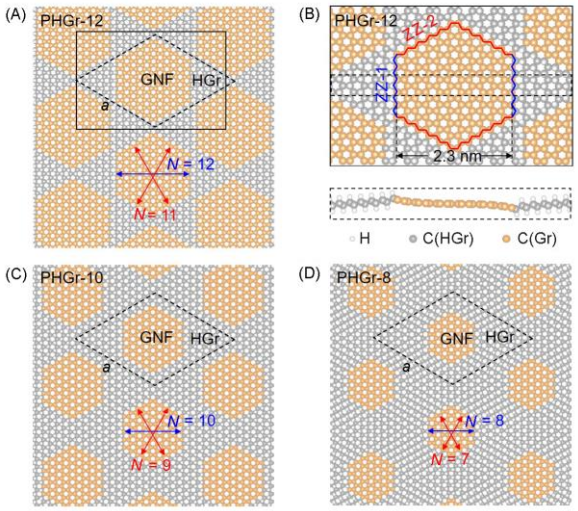

Fig.1 Atomic structures of different sized GNF arrays embedded in PHGrs

The black dotted rhombuses mark the primitive cells. (A) A large-scaled PHGr-12 monolayer consists of two parts: hydrogenated graphene(graphane, HGr) and hexagonal graphene nano flakes(GNFs); (B) the top view(up) and side view (down) of the zoom-in atomic structure of PHGr-12 in the black rectangle in (A)[there are two kinds of zigzag boundaries between HGr and GNF, zigzag 1 (ZZ-1) and zigzag 2(ZZ-2), marked by red and blue zigzag lines, respectively, the distance between two ZZ-1 boundaries is 2.3 nm(N=12)]; the atomic structure of PHGr with small size of GNFs: PHGr-10(C) and PHGr-8(D) with N being the number of carbon atoms on the ZZ-2 boundaries of the GNF.

3.2 Antiferromagnetism of GNF Arrays

According to the symmetry of hexagonal GNF, the electron density differences of spin up($\Delta\rho\uparrow$) and spin down($\Delta\rho\downarrow$) electrons marked by magenta and cyan, respectively, of four

https://doi.org/10.1007/s40242-021-1163-x

possible magnetic states, namely antiferromagnetism-1(AFM-1), antiferromagnetism-2(AFM-2), ferromagnetism(FM) and paramagnetism(PM), are shown in Fig.2(A)—(D). In AFM-1, the spin-up and spin-down electrons distribute separately on opposite ZZ-1 boundaries of each GNF with a little extension to the neighboring carbon atoms. In AFM-2 state, the electron distribution is similar with that in AFM-1 state, but the spin direction of the corner carbon atoms is different from that on the boundaries. The most energetically stable state is AFM-1, while the total energy of AFM-2, FM and PM states are 0.16, 0.14 and 0.49 eV higher than that of AFM-1 state, respectively. The ground state(AFM-1) has a similar spin-polarized state to the AFM states of ZGNR[8,10,15] and bow-tie-shaped GNF[11,18], rather than non-spin-polarized state of pure hexagonal GNF[11].

The spin-polarized density of states(DOSs) of four magnetic states(AFM-1, AFM-2, FM and PM) are presented in Fig.2(E)—(H). The band gaps of PHGr-12 in AFM-1 and AFM-2 states are 0.37 and 0.25 eV, respectively, while PHGr-12 in FM and PM states are metallic. It indicates that the AFM-FM transition can be identified as a semiconductor-metal transition, similar to the width-dependent AFM-FM (semiconductor-metal) transition in ZGNRs. Therefore, one can expect that the PHGr would undergo a semiconductor-metal when a suitable magnetic field is applied.

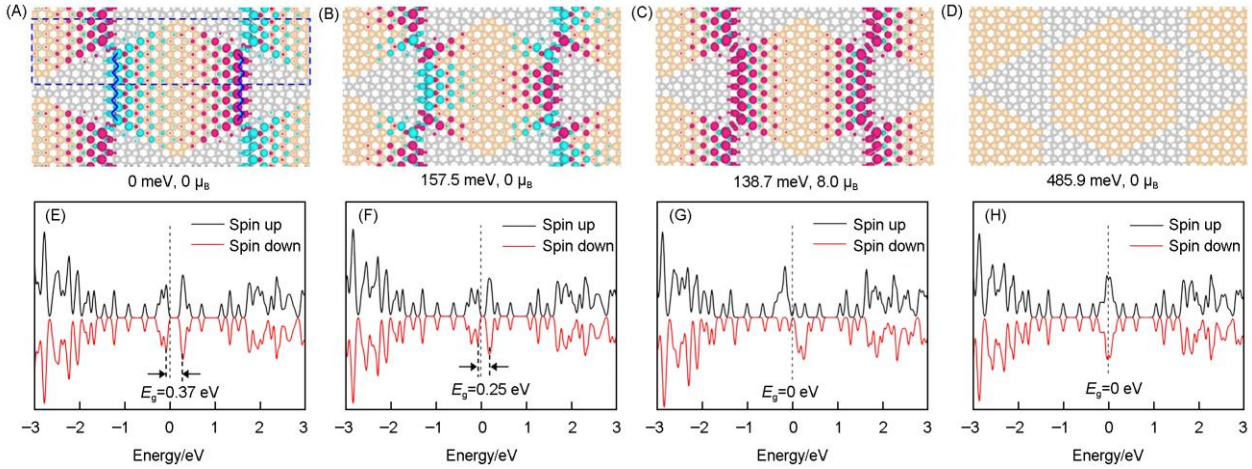

Fig.2 Spin-polarized electron density difference($\rho\uparrow-\rho\downarrow$) and total DOS of PHGr-12 with different magnetic orders

The isosurface value is 0.0016 e/bohr^3. The isosurfaces of $\Delta\rho\uparrow$ and $\Delta\rho\downarrow$ are marked by magenta and cyan, respectively. (A) The spatial distribution of the spin-polarized electron density difference for the antiferromagnetic ground state, AFM-1, which is similar to the spin configuration of ZGNR(the magnetic moment of 0.22 μ_B is localized around the unhydrogenated carbon atoms on the ZZ-1 boundaries. The magnetism decay gradually from the boundaries to the center of GNFs); (B—D) the spatial distribution of the spin-polarized electron density difference for other spin configurations: antiferromagnetic(AFM-2), ferromagnetic(FM) and nonmagnetic(NM), respectively; (E—H) spin-polarized total DOS of PHGr-12 with different magnetic orders[the band gaps of AFM-1 and AFM-2 states are 0.37 and 0.25 eV, respectively, while FM and PM states are metallic, the relative total energies and the total magnetic moments μ are presented at the bottom of images (A—D)].

3.3 Origin of the Spin-polarized Boundary States of GNF Arrays

The projected densities of states(PDOS) in Fig.3 are used to further illustrate the origin of the spin-polarized boundary states in AFM-1. The magnetic ordering of the AFM-1 configuration is similar to that in ZGNR and bow-tie-shaped GNF. The largest magnetic moments of ±0.22 μ_B are localized around the carbon atoms without H on the ZZ-1 boundaries, such as C_1, C_3 and C_5 marked in black and red in Fig.3(A). The spin-polarized PDOSs projected on the in-plane p orbitals (p_x and p_y, marked by red line) and out-of-plane p orbital (p_z, marked by blue line) on the carbon atoms labeled in Fig.3(A) are plotted in Fig.3(B). The AFM state originates from an antiparallel alignment of spins on the two ZZ-1 boundaries. The PDOS indicates that the spin up(down) electrons located at the right(left) boundary is contributed by the out-of-plane orbital, p_z orbital, splitting near the Fermi level. Additionally,

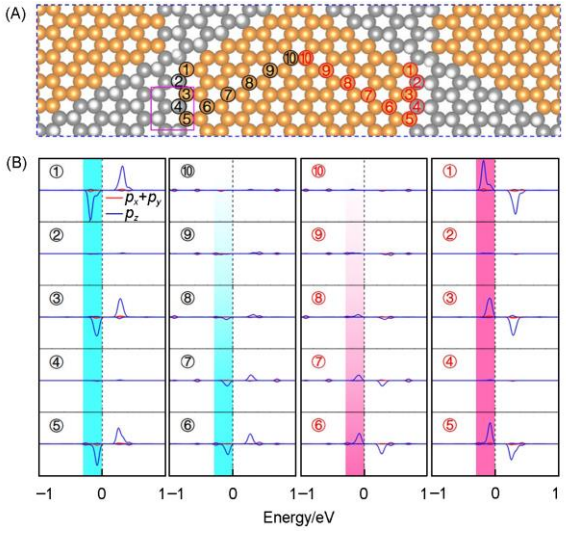

Fig.3 Spin-polarized boundary states in PHGr-12

(A) The enlarged atomic structure in the blue dotted rectangle in Fig.2(A); (B) spin-polarized PDOS of the in-plane p orbitals(p_x and p_y, marked by red line) and out-of-plane p orbital(p_z, marked by blue line) of the carbon atoms numbered in (A). The cyan and magenta backgrounds distinguish the spin down and spin up nature.

https://doi.org/10.1007/s40242-021-1163-x

the spins of ZZ-1 boundary-atoms couple with the neighboring atoms in the same sublattices in ferromagnetic ordering throughout GNF. Meanwhile, the magnetic moment decays from the ZZ-1 boundaries(C_1, C_3, C_5) to the center of GNF(C_6—C_{10}).

On ZZ-1 boundaries, there are two types of carbon atoms: $C_1/C_3/C_5$ without H adsorption, and C_2/C_4 with H adsorption. The $C_1/C_3/C_5$ atom is in an sp^2 hybridization state, while the C_2/C_4 atom is in an sp^3 hybridization state. Fig.4(A) shows a zoom-in structure of the top and side views[the magenta rectangle part in Fig.3(A)] of the ZZ-1 boundary. The spin-polarized PDOSs[Fig.4(B)] for the H, C_4, and C_5 atoms labeled in Fig.4(A) show overlaps around the Fermi level between H atom and the sp^2-hybridized C_5 atom(the green-shaded area). The overlaps indicate that the spin polarization is mainly due to the interaction between the H and C_5 atoms rather than that between the H atom and the sp^3-hybridized C_4 atom(the yellow-shaded area).

To check the robustness of AFM-1 state of HGr, we construct similar PHGr models with smaller-sized GNFs, such as PHGr-10 and PHGr-8 displayed in Fig.1(C) and (D), whose widths of GNF are 1.8 nm(N=10) and 1.4 nm(N=8), respectively. Spin polarization calculations show that there are only AFM-1 and FM states in PHGr-10 and AFM-1 and PM states in PHGr-8. In Table 1, the most energetically stable state in PHGr-10 and PHGr-8 are AFM-1 state. The spatial distributions of spin electron density($\rho\uparrow-\rho\downarrow$) of PHGr-10 and PHGr-8 in ground state(AFM-1) are shown in Fig.5(A) and (B) with the isosurface value of 0.0016 e/bohr^3. As expected, both PHGr-10 and PHGr-8 possess the similar spin electron density distribution with that in PHGr-12, indicating AFM-1 state is robust when the size of GNF varies from 1.4 nm to 2.3 nm. The total DOSs in Fig.5(C) and (D) demonstrate that PHGr-10 and PHGr-8 are both semiconductors with a band gap of 0.33 eV.

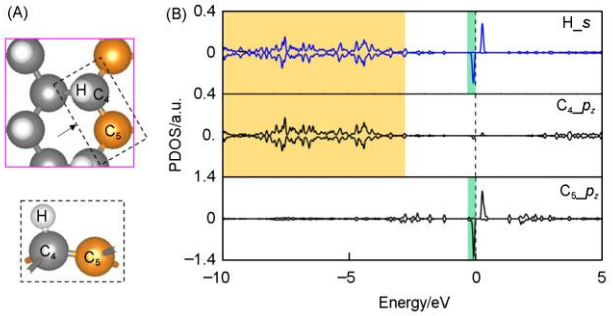

Fig.4 PDOS of atoms on ZZ-1 boundary

(A) The top(upper panel) and side(lower panel) views of a zoom in of the ZZ-1 boundary marked by a magenta dotted rectangle in Fig.3(A); (B) the spin-polarized PDOSs for H, C_4 and C_5 atoms in (A) showing the contribution from different orbitals.

Table 1 Total energy(E_{Total}), total magnetic moment(μ_{Total}), the largest magnetic moment on single C atom(μ_{Max}) and the energy gap(E_g) of PHGr-12, PHGr-10 and PHGr-8 at AFM-1, AFM-2, FM and PM states

Layer	State	E_{Total}/eV	μ_{Total}/μ_B	μ_{Max}/μ_B	E_g/eV
PHGr-12	AFM-1	0	0	±0.22	0.37
	AFM-2	0.16	0	±0.22	0.25
	FM	0.14	8.02	0.23	0.13
	PM	0.49	0	0	0.06
PHGr-10	AFM-1	0	0	±0.21	0.33
	FM	0.16	5.91	0.22	0.10
PHGr-8	AFM-1	0	0	±0.11	0.33
	PM	0.01	0	0	0.27

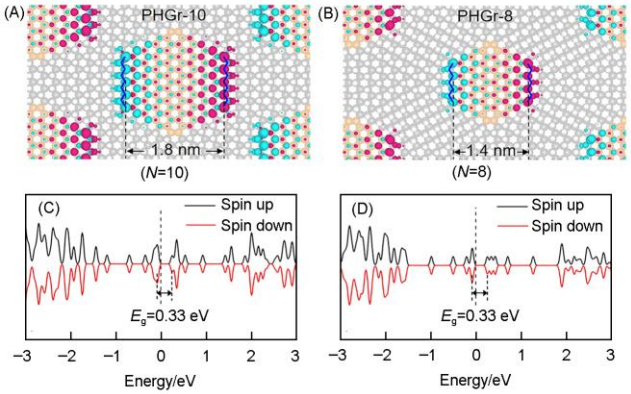

Fig.5 Spin configuration of antiferromagnetic ground state and spin-polarized total DOSs of PHGr-10 and PHGr-8

(A, B) The distribution of spin in PHGr-10 and PHGr-8 with GNFs, whose widths are 1.8 nm(N=10)(A) and 1.4 nm(N=8)(B), respectively(the isosurface value is 0.0016 e/bohr^3; (C, D) spin-polarized total DOSs of PHGr-10 and PHGr-8, respectively with magnetic orders of AFM-1(the band gaps of PHGr-10 and PHGr-8 with the AFM-1 state are both 0.33 eV).

3.4 Selective Adsorption of Au Atoms on GNFs for Catalyzing H_2 Dissociation

Patterned 2D materials are known as templates for selective adsorption of nanoparticles or atoms[30,31]. Here we choose a single Au atom, which is active for H_2 dissociation[32], thus may promote the local hydrogenation of graphene. First of all, a single Au atom prefers to be adsorbed on ZZ-1 boundaries[*e.g.*, C_5 in Fig.3(A) and labeled by the yellow star in Fig.6(A)]. The adsorption energies of an Au atom on top of C_5 are 0.78 and 0.76 eV lower than those on the first[marked by a blue star in Fig.6(A)] and the second(marked by a magenta star) neighboring carbon atoms, respectively. The other adsorption sites, bridge sites marked by black spots and hollow sites marked by black squares, are found unstable for holding Au atoms. The spin-polarized edge states assist the selective adsorption of Au atoms and the adsorbed Au atoms benefit the H_2 adsorption and further dissociation discussed as follows.

Then, we check the reaction activity of the Au adatom on PHGr for a H_2 dissociation reaction. The relative total energies of gas state, initial state(IS), transition state(TS), final state 1 (FS_1) and final state 2(FS_2) are shown in Fig.6(B). The overall reaction contains both H_2 dissociation process and graphene hydrogenation process, and is exothermic. In the adsorption

https://doi.org/10.1007/s40242-021-1163-x

process, H_2 molecule gets gradually close to the Au atom from gas state to IS. The H—H bond length increases slightly from 0.077 nm to 0.086 nm. In H_2 dissociation process, one H atom gradually moves to the nearest sp^2-carbon atom on ZZ-1 boundary by overcoming an energy barrier of 0.74 eV. Finally, the other H atom leaves Au and bonds to the sp^2 carbon nearby(FS_2). Compared to the barrier of hydrogenation of graphene without Au(3.3 eV)[33], the barrier with an Au adatom has been significantly decreased. The selective adsorption of single atoms, Au in this case and can extend to Pt etc., promotes the hydrogenation of graphene on boundaries, thus potentially guides the growth of hydrogenated graphene in a regular shape.

To explore the binding nature of Au on GNFs and the effect of H_2 adsorption on Au atom on the adsorption of Au, we calculated the spin-polarized PDOSs for the carbon atoms on the boundary without[Fig.7(A)] and with[Fig.7(B)] Au adsorption. Without Au adsorption, the spin-polarized state is contributed by the *p* orbitals of C. With Au adsorption, the *s* and *d* orbitals of Au(the black and green lines) interact with *p* orbitals of C(the blue line), which wipes out the local spin polarization. The length of Au—C bond is 0.21 nm, indicating a chemical adsorption. We also calculated the spin-polarized PDOSs for the Au atoms without[Fig.7(C)] and with[Fig.7(D)] H_2 adsorption. We found that the H_2 adsorption slightly affects the electronic states of the Au atom. The inserted side view of the atomic structure shows that the lengths of Au—C bond without and with H_2 adsorption are consistent. The density of

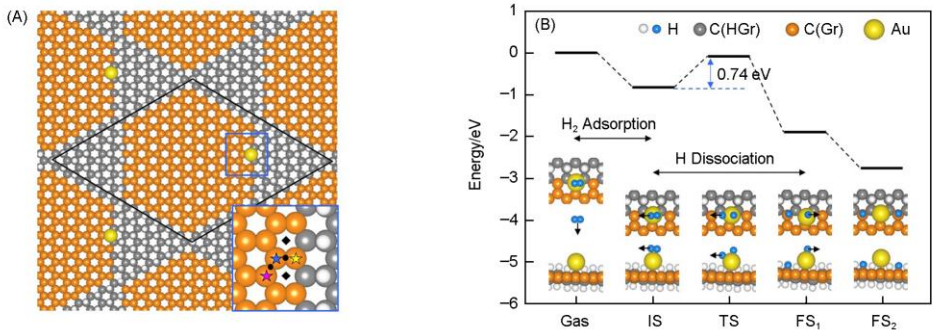

Fig.6 Selective adsorption of Au atoms on PHGr and energy diagram of hydrogen dissociation

(A) Selective adsorption of gold single atoms on the boundary of GNF and graphene in PHGr-12. The inset is the enlarged image of the region in the blue square without Au adatom. We consider different adsorption sites, atop, bridge and hollow at the boundary marked by star, dot and square, respectively. The yellow star marks the most energetically stable adsorption site; (B) potential energy landscape and the top view and side view of the H_2 adsorption and dissociation processes. After hydrogen molecule is adsorbed on the Au atom(IS), one of the H atoms separates from Au atom and is adsorbed on neighboring sp^2 carbon(FS_1). The dissociation barrier is 0.74 eV. FS_2 is the subsequent state after H_2 dissociation, in which two H atoms bond to two neighboring sp^2 C atoms at the boundary.

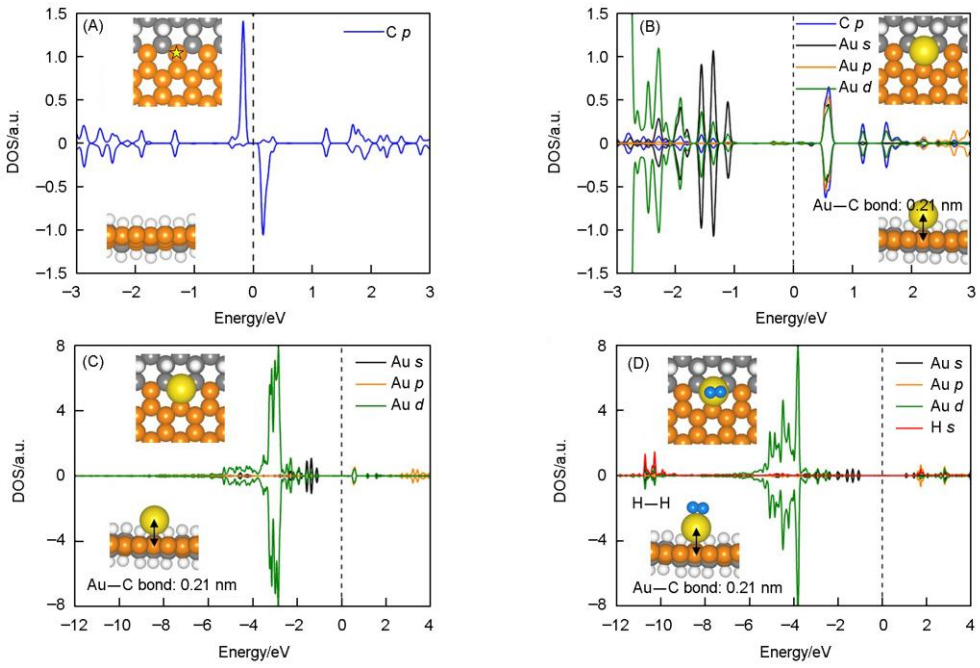

Fig.7 Spin-polarized PDOSs for C, Au, H atoms in GNF

(A) C atom on the boundary of the pristine GNF; (B) C atom on the boundary and the adsorbed Au atom in the GNF-Au system; (C) the same system as (B) in an enlarged energy range; (D) the adsorbed Au atom and the adsorbed H_2 in the GNF-Au-H_2 system. The insets are the top view and side view of the corresponding atomic structures.

https://doi.org/10.1007/s40242-021-1163-x

states of H_2(the red line) is mainly localized on the deep energy level, below the Fermi level for more than 10 eV, indicating that the H—H bond remains, and *s* orbital of H_2 couples with the *d* orbitals of Au.

4 Conclusions

In summary, we have predicted a new partially hydrogenated graphene with an embedded GNFs array. PHGr is a semiconductor in an antiferromagnetic ground state. The antiferromagnetic boundary states localized on the boundaries of GNF and HGr are due to the coupling between the sp^2 carbons at the boundary and the H atoms on the neighboring sp^3 carbon atom. The antiferromagnetism and semiconducting are robust when the size of GNF varies from 1.4 nm to 2.3 nm. The GNF array with an antiferromagnetic boundary state can be used as a template for selective adsorption of Au adatoms to assist further hydrogenation for GNF. Therefore, the PHGr, an antiferromagnetic semiconductor, is highly expected to be used in carbon-based spintronic devices and as a template for catalyst.

Acknowledgements

This work was supported by the National Natural Science Foundation of China (No.61888102), the National Key Research and Development Projects of China (Nos.2016YFA0202300, 2018YFA0305800), and the Strategic Priority Research Program of the Chinese Academy of Sciences, China(No.XDB30000000). Computational resources were provided by the National Supercomputing Center in Tianjin.

Conflicts of Interest

The authors declare no conflicts of interest.

References

[1] Geim A. K., Novoselov K. S., *Nat. Mater.*, **2007**, *6*(3), 183
[2] Castro Neto A. H., Guinea F., Peres N. M. R., Novoselov K. S., Geim A. K., *Rev. Mod. Phys.*, **2009**, *81*(1), 109
[3] Avouris P., *Nano Lett.*, **2010**, *10*(11), 4285
[4] Tan Y., Xia X.-S., Liao X.-L., Li J.-B., Zhong H.-H., Liang S., Xiao S., Liu L.-H., Luo J.-H., He M.-D., Chen L.-Q., *Carbon*, **2020**, *157*, 724
[5] Li Y. Y., Chen M. X., Weinert M., Li L., *Nat. Commun.*, **2014**, *5*(1), 4311
[6] Dutta S., Pati S. K., *J. Mater. Chem.*, **2010**, *20*(38), 8207
[7] Nakada K., Fujita M., Dresselhaus G., Dresselhaus M. S., *Phys. Rev. B*, **1996**, *54*(24), 17954
[8] Magda G. Z., Jin X., Hagymási I., Vancsó P., Osváth Z., Nemes-Incze P., Hwang C., Biró L. P., Tapasztó L., *Nature*, **2014**, *514*(7524), 608
[9] Fujita M., Wakabayashi K., Nakada K., Kusakabe K., *J. Phys. Soc. JPN*, **1996**, *65*(7), 1920
[10] Son Y.-W., Cohen M. L., Louie S. G., *Nature*, **2006**, *444*(7117), 347
[11] Wang W. L., Yazyev O. V., Meng S., Kaxiras E., *Phys. Rev. Lett.*, **2009**, *102*(15), 157201
[12] Yazyev O. V., Katsnelson M. I., *Adv. Funct. Mater.*, **2012**, *2*, 71
[13] Siemion F., Peter E. J., Sachsb H., *Croat. Chem. Acta*, **2005**, *78*, 195
[14] Lieb E. H., *Phys. Rev. Lett.*, **1989**, *62*(10), 1201
[15] Dutta S., Pati S. K., *J. Phys. Chem. B*, **2008**, *112*(5), 1333
[16] Ruffieux P., Wang S., Yang B., Sánchez-Sánchez C., Liu J., Dienel T., Talirz L., Shinde P., Pignedoli C. A., Passerone D., Dumslaff T., Feng X., Müllen K., Fasel R., *Nature*, **2016**, *531*(7595), 489
[17] Shinde P. P., Liu J., Dienel T., Gröning O., Dumslaff T., Mühlinghaus M., Narita A., Müllen K., Pignedoli C. A., Fasel R., Ruffieux P., Passerone D., *Carbon*, **2021**, *175*, 50
[18] Mishra S., Beyer D., Eimre K., Kezilebieke S., Berger R., Gröning O., Pignedoli C. A., Müllen K., Liljeroth P., Ruffieux P., Feng X., Fasel R., *Nat. Nanotechnol.*, **2020**, *15*(1), 22
[19] Li Y., Zhang W., Morgenstern M., Mazzarello R., *Phys. Rev. Lett.*, **2013**, *110*(21), 216804
[20] Chen H., Que Y., Tao L., Zhang Y.-Y., Lin X., Xiao W., Wang D., Du S., Pantelides S. T., Gao H.-J., *Nano Res.*, **2018**, *11*(7), 3722
[21] Li Y., Zhou Z., Cabrera C. R., Chen Z., *Sci. Rep.*, **2013**, *3*, 2030
[22] Chen H., Bao D.-L., Wang D., Que Y., Xiao W., Qian G., Guo H., Sun J., Zhang Y.-Y., Du S., Pantelides S. T., Gao H.-J., *Adv. Mater.*, **2018**, *30*(32), 1801838
[23] Blöchl P. E., *Phys. Rev. B*, **1994**, *50*(24), 17953
[24] Kresse G., Joubert D., *Phys. Rev. B*, **1999**, *59*(3), 1758
[25] Kresse G., Furthmüller J., *Phys. Rev. B*, **1996**, *54*(16), 11169
[26] Kresse G., Furthmüller J., *Comput. Mater. Sci.*, **1996**, *6*(1), 15
[27] Monkhorst H. J., Pack J. D., *Phys. Rev. B*, **1976**, *13*(12), 5188
[28] Henkelman G., Uberuaga B. P., Jónsson H., *J. Chem. Phys.*, **2000**, *113*(22), 9901
[29] Henkelman G., Jónsson H., *J. Chem. Phys.*, **2000**, *113*(22), 9978
[30] Lin X., Lu J. C., Shao Y., Zhang Y. Y., Wu X., Pan J. B., Gao L., Zhu S. Y., Qian K., Zhang Y. F., Bao D. L., Li L. F., Wang Y. Q., Liu Z. L., Sun J. T., Lei T., Liu C., Wang J. O., Ibrahim K., Leonard D. N., Zhou W., Guo H. M., Wang Y. L., Du S. X., Pantelides S. T., Gao H. J., *Nat. Mater.*, **2017**, *16*(7), 717
[31] Liu Z.-L., Lei B., Zhu Z.-L., Tao L., Qi J., Bao D.-L., Wu X., Huang L., Zhang Y.-Y., Lin X., Wang Y.-L., Du S., Pantelides S. T., Gao H.-J., *Nano Lett.*, **2019**, *19*(8), 4897
[32] Righi G., Magri R., Selloni A., *J. Phys. Chem. C*, **2019**, *123*(15), 9875
[33] Miura Y., Kasai H., Diño W., Nakanishi H., Sugimoto T., *J. Appl. Phys.*, **2003**, *93*(6), 3395